Environmental Science & Technology

Article

pubs.acs.org/est

Transient Secondary Organic Aerosol Formation from Limonene Ozonolysis in Indoor Environments: Impacts of Air Exchange Rates and Initial Concentration Ratios

Somayeh Youssefi and Michael S. Waring*

Department of Civil, Architectural and Environmental Engineering, Drexel University, 3141 Chestnut Street, Philadelphia, Pennsylvania 19104, United States

ABSTRACT: Secondary organic aerosol (SOA) results from the oxidation of reactive organic gases (ROGs) and is an indoor particle source. The aerosol mass fraction (AMF), a.k.a. SOA yield, quantifies the SOA forming potential of ROGs and is the ratio of generated SOA to oxidized ROG. The AMF depends on the organic aerosol concentration, as well as the prevalence of later generation reactions. AMFs have been measured in unventilated chambers or steady-state flow through chambers. However, indoor settings have outdoor air exchange, and indoor SOA formation often occurs when ROGs are transiently emitted, for instance from emissions of cleaning products. Herein, we quantify "transient AMFs" from ozonolysis of pulse-emitted limonene in a ventilated chamber, for 18 experiments at low (0.28 h^{-1}), moderate (0.53 h^{-1}), and high (0.96 h^{-1}) air exchange rates (AER) with varying initial ozone−limonene ratios. Transient AMFs increased with the amount of ROG reacted; AMFs also increased with decreasing AERs and increasing initial ozone−limonene ratios, which together likely promoted more ozone reactions with the remaining exocyclic bond of oxidized limonene products in the SOA phase. Knowing the AER and initial ozone−limonene ratio is crucial to predict indoor transient SOA behavior accurately.

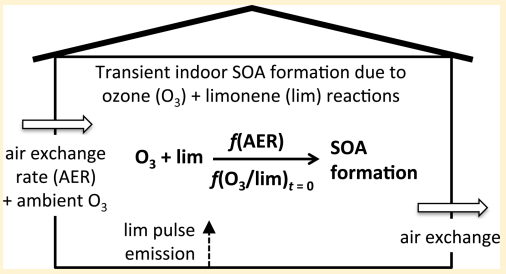

INTRODUCTION

Cooking,[1] smoking,[2] and resuspension[3] are aerosol emission sources indoors.[4] Another source is the secondary organic aerosol (SOA) formation that results from the oxidation of reactive organic gases (ROGs) by ozone (O_3), hydroxyl radicals (OH), or nitrate radicals (NO_3). ROG oxidation forms gaseous products, some of which have low vapor pressures and generate SOA by partitioning to available aerosols or self-nucleating.[5] SOA can contribute up to 70% of urban organic aerosols,[6,7] and indoors, ozone and terpenoid reactions generate SOA[8−15] that can meaningfully influence organic aerosol concentrations.[16] Indoor ozone from outdoor-to-indoor transport is typically at ∼20−70% of outdoor concentrations,[17,18] and it may be emitted indoors from appliances[19] or equipment.[20] Indoor terpenoid concentrations are mostly due to emissions from products such as air fresheners,[15,21] perfumes, and cleaning agents.[22] The dominant indoor terpenoid is limonene; it is the focus of this article and may reach up to 50 ppb in residences for 48-h integrated samples,[23] or up to 1000 ppb during product use.[21]

SOA is composed of numerous ROG oxidation products, and despite many studies,[5,14,24−29] the exact pathways of SOA formation and growth remain uncertain. To parametrize formation, researchers use the "aerosol mass fraction" (AMF),[30,31] which is also called the "SOA yield" and is the ratio of SOA mass produced, ΔC_{SOA} ($\mu g/m^3$), to ROG mass reacted, ΔROG ($\mu g/m^3$).[12,30] Unlike molar yields for gases, the AMF for the oxidation of a particular ROG is not constant. The AMF framework developed by Odum et al.[32] uses the gas-particle partitioning theory of Pankow[33,34] to describe the dependence of the AMF on the total organic aerosol concentration, C_{OA} ($\mu g/m^3$):

$$\text{AMF} = \frac{\Delta C_{SOA}}{\Delta \text{ROG}} = \sum_i \alpha_i \left(1 + \frac{c_i^*}{C_{OA}}\right)^{-1} \quad (1)$$

which accounts for the summed contributions of mutliple oxidation products; α_i is the mass-based yield of product i, and c_i^* ($\mu g/m^3$) is the effective gas-phase saturation concentration of product i. AMF experiments are fit with eq 1 by letting both α_i and c_i^* parameters vary for a certain number of hypothetical products (usually one or two), or with the "volatility basis set" approach, which constrains c_i^* at logarithmic intervals (e.g., 0.1 to 1000 $\mu g/m^3$) and fits α_i only at those c_i^*'s.

Experiments to measure AMFs are often performed in batch reactors (i.e., unventilated chambers) to mimic the atmosphere.[32,35−46] For instance, Zhang et al.[47] measured unit density normalized "batch AMFs" for limonene ozonolysis ranging from 0.05 to 1.1 for a C_{OA} of ∼0.1−1000 $\mu g/m^3$, and Presto and Donahue[48] measured AMFs for α-pinene ozonolysis of 0.01−0.35 over the same C_{OA} range. These experiments were performed under ozone-excess conditions to ensure full ROG oxidation, which is an important point for limonene, because it

Received: February 26, 2014
Revised: May 5, 2014
Accepted: June 18, 2014
Published: June 18, 2014

   dx.doi.org/10.1021/es5009906 | Environ. Sci. Technol. 2014, 48, 7899−7908

is doubly unsaturated with endo- and exocyclic double bonds. For ozone-limited conditions, the endo- bond is preferentially attacked by ozone,[47] resulting in lower AMFs that resemble those from ozonolysis of α-pinene or limona ketone,[49] which both have single endo- double bonds. Under low NO_x ($NO + NO_2$) conditions, the exo- bond is oxidized within the aerosol rather than in the gas phase; under high NO_x conditions, this exo- bond oxidation can occur in the gas phase.[47,50]

Indoor environments have air exchange with the outdoor air; e.g., U.S. residences[51] typically have air exchange rates (AER) of ~0.2 to 1.5 h^{-1} and offices[52] of ~0.50 to 5.9 h^{-1}. Therefore, experimental chambers operated as continuously mixed flow reactors (CMFR) better represent indoor spaces than do batch reactors. Higher AERs may reduce SOA formation[53] because they likely reduce residence times during which later generation reactions can occur and flush products from the system with exhaust air. To date, CMFRs have been used to measure "steady state AMFs," in which reactants were continuously introduced into chambers,[7,10,54−56] though the AER has not been varied systematically to quantify its impact on AMFs. Chen and Hopke[55] measured limonene ozonolysis steady state AMFs at an AER = 0.67 h^{-1}; at similar C_{OA}, they were lower in magnitude than batch AMFs from Zhang et al.,[47] though the Chen and Hopke[55] AMFs were for much lower ozone−limonene ratios.

Indoor SOA generation often occurs when ROGs are transiently emitted, for instance from pulse emissions of products such as cleaners.[21] We are unaware of any studies that have determined "transient AMFs" for dynamic reactant combinations in systems with air exchange. Therefore, we explored SOA formation from a nonreplenished combination of limonene and ozone in a CMFR system. Limonene was used because it has the highest AMFs of any monoterpene and is prevalent indoors, and its double unsaturation makes it interesting because air exchange time scales may compete with secondary exo- bond oxidation time scales. To quantify impacts of AER and ozone−limonene ratios, we performed 18 experiments at low (0.28 h^{-1}), moderate (0.53 h^{-1}), and high (0.96 h^{-1}) AERs at different initial ozone−limonene ratios. Using a dynamic indoor SOA formation framework we previously developed,[57] transient AMFs were parametrized as functions of variables useful for predicting SOA formation in indoor models.

METHODOLOGY

Experimental Method. Experiments were performed in the CMFR system in Figure 1, which uses a stainless steel chamber of volume = 1 m^3 and surface area = 6 m^2. A zero air generator (Environics 7000) supplied dehumidified, particle-filtered, clean air (SO_2, NO_x, O_3 < 0.5 ppb; CO, hydrocarbons < 0.02 ppm) as the primary air stream at controlled rates (Aarlborg GFC171S), which was split into eight entry points within the chamber to ensure mixing, as verified by tracer tests. Ozone was introduced into the chamber by a calibration source (2B Technologies, 306) at desired initial concentrations, and a powerful generator (Absolute Ozone, Nano) produced ozone at ppm levels to clean the chamber between experiments. Limonene was pulsed into the chamber by using a syringe pump (New Era Pump Systems 300) to deliver a liquid solution of limonene (Sigma-Aldrich, 98%) in methanol (Sigma-Aldrich, 99.9%) to a heated injection area with a separate clean air stream (volume ratio of methanol-to-limonene = 49:1).

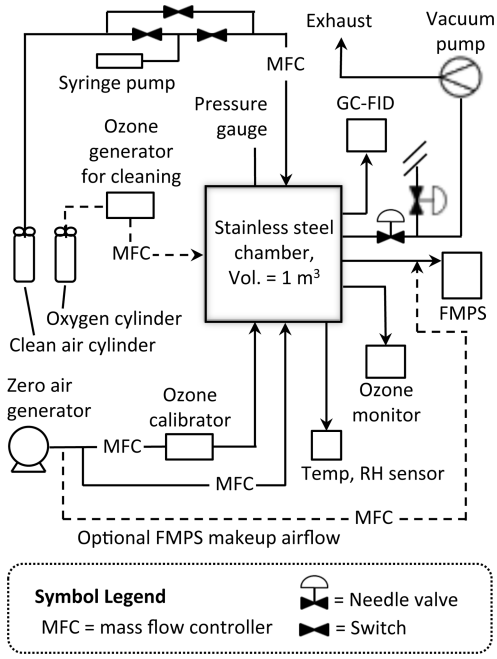

Figure 1. Schematic of continuous mixed flow reactor (CMFR) system with stainless steel chamber (volume = 1 m^3) to measure SOA formation due to transient limonene ozonolysis. Instruments and the method of chamber operation are described in the text.

Relative humidity (RH), temperature (Onset HOBO U12), and ozone (2B Technologies 205, uncertainty > of 1 ppb or 2%, flow = 1.5 L/min) were measured each minute. Artifacts in ozone measurement may exist at high limonene concentrations, but this was within instrument noise for our experiments, based on previous characterizations. The chamber limonene was measured every ~20 min using gas chromatograph−flame ionization detection (GC-FID), equipped with a pump (1 min samples), Tenax adsorption, and thermal desorption system (SRI GC8610C). A calibration curve for limonene was prepared by drawing samples through the sampling system from 3 L Tedlar bags with amounts of limonene in a volume of 2.5 L of clean air (R^2 = 0.99). Limonene measurement had an uncertainty of 8%, equal to two standard deviations of calibration standards. The chamber particle size distribution and volume loading were measured over 1 min averages using a Fast Mobility Particle Sizer, FMPS (TSI 3091, flow = ~8 L/min). For low and medium AERs, the sum of instrument flows exceeded the chamber flow. For these cases, the FMPS flow was diluted by the necessary amount with make up flow from the zero air generator; FMPS concentrations were adjusted to account for this dilution.

We performed 18 experiments with six each at low, moderate, and high AERs with varying initial ozone−limonene ratios without seed particles, at room temperature and low RH so that we could compare our results to others using similar conditions.[47,49,55] Between experiments, the chamber was cleaned with ~250 ppm ozone, followed by clean air flushing. After that, ozone was generated to reach its target initial concentration. Then, an amount of limonene solution was injected to the chamber for 30 s to generate limonene in the chamber near its desired target concentration. Flows were measured (Sensidyne Gilian Gilibirator) at the end of the experiments. Chamber pressure was maintained at 25 Pa relative to surroundings. The SOA deposition rate was

Table 1. Experimental Conditions and Results for 18 Experiments Measuring Transient Secondary Organic Aerosol (SOA) Formation Due to Limonene Ozonolysis

expt. ID[a]	air exchange rate (h^{-1})	RH[b] (%)	temp.[c] (°C)	initial ozone (ppb)	initial limonene (ppb)	surface deposition rate (h^{-1})	max SOA mass[d] ($\mu g/m^3$)	max SOA number[d] (#/cm^3)	GM of max[d] (nm)	GSD of max[d] (−)
moderate air exchange rate experiments										
E1	0.53	3	23	45	422	0.15	66	318 000	37	1.5
E2	0.52	10	23	45	119	0.32	33	288 000	31	1.6
E3	0.52	9	23	45	67	0.28	17	107 000	35	1.5
E4	0.53	6	24	295	20	0.19	53	149 000	40	1.7
E5	0.53	10	24	195	30	0.25	39	165 000	46	1.4
E6	0.53	6	23	94	35	0.32	21	108 000	50	1.4
low air exchange rate experiments										
E7	0.26	10	23	41	428	0.43	55	137 000	65	1.5
E8	0.27	17	28	46	275	0.36	55	93 000	65	1.5
E9	0.31	7	23	45	118	0.34	42	155 000	35	1.5
E10	0.28	0	23	300	243	0.23	330	517 000	70	1.5
E11	0.30	10	23	192	72	0.18	116	313 000	64	1.5
E12	0.26	0	23	95	122	0.21	83	162 000	55	1.5
high air exchange rate experiments										
E13	0.95	0	23	45	663	0.47	16	86 000	41	1.5
E14	0.95	0	23	45	131	0.10	11	23 000	72	1.4
E15	0.96	0	23	45	67	0.45	5.4	28 000	55	1.5
E16	0.96	0	22	295	58	0.16	40	265 000	35	1.5
E17	0.95	0	23	195	34	0.18	24	99 000	37	1.5
E18	0.97	0	23	95	42	0.24	12	71 000	37	1.5

[a]Experiment identification number. [b]RH = relative humidity. [c]Temp. = temperature. [d]The maximum SOA mass and number concentrations occurred at different times in the experiments. The number maximum always occurred prior to the mass maximum, and the GM (geometric mean) and GSD (geometric standard deviation) are for the maximum number concentration.

determined with a first order decay function once formation ceased. Though ozone and limonene reactions generate OH,[58−61] we did not use OH scavengers; however, the methanol used as the solvent reduced OH but this had little effect on formation (discussed below).

AMF Calculation Method. We calculated unit density AMFs, which used the SOA volume loading from the FMPS and assumed a particle density of 1 g/cm^3, so that our results could be compared to others[47,49] who did the same. To calculate AMF parameters, knowing the initial concentration of the parent ROG was necessary. With our apparatus, we could not measure the limonene concentration at time zero, so we estimated the initial concentration of limonene by using an Euler solution for limonene decay due to ozonolysis (reaction rate constant of 0.0183 $ppb^{-1}\ h^{-1}$)[62] and air exchange. Using measured ozone concentrations, we solved for the initial limonene concentration for each experiment by calculating the one that minimized the sum of least squared difference between measured limonene concentrations and those predicted with the Euler solution, at times of GC-FID measurements. After finding the initial limonene concentration, the predicted limonene concentrations at each minute were also determined.

In batch systems, the AMF is the ratio of the formed SOA mass (wall-loss corrected) and the converted ROG mass,[32,35−37,40,42−45] and in steady state systems, it is the ratio of the steady state rate of formed SOA (wall-loss corrected) and rate of ROG conversion.[7,54,55] However, our system had air exchange, and reactants were not replenished, requiring a dynamic framework. We followed method SOA-M2 from Youssefi and Waring[57] that describes the SOA concentration as a function of the amount of ROG oxidation products in the chamber over time and is a modified form of the framework in Kroll and Seinfeld,[63] which predicts SOA as a function of ΔROG for batch systems. We recognize that the ΔROG in a batch system is proportional to the increase in the products that may partition to form SOA mass and instead track the concentration of a hypothetical product dROG, C_{dROG} ($\mu g/m^3$), which is a lumped compound representing limonene oxidation products in the chamber at any time. In batch reactors, C_{dROG} = ΔROG, but in transient CMFR systems, C_{dROG} < ΔROG.

Youssefi and Waring[57] derived an equation to predict C_{dROG} in a dynamic system by substituting $C_{SOA} = (AMF \cdot C_{dROG})$ into a differential equation for C_{SOA} that considered formation due to ozonolysis of one terpenoid only, computing the derivative of $d(AMF \cdot C_{dROG})/dt$, and then rearranging, so that

$$\frac{dC_{dROG}}{dt} = kC_{O3}C_{lim}\Gamma_{lim} - \left(\lambda + \beta_{SOA} + \frac{1}{AMF}\frac{d(AMF)}{dt}\right)C_{dROG} \quad (2)$$

where t (h) is time; k ($ppb^{-1}\ h^{-1}$) is the reaction rate constant between ozone and limonene; C_{O3} and C_{lim} (ppb) are the ozone and limonene mole fractions, respectively; Γ_{lim} is a conversion factor to change units from ppb to $\mu g/m^3$ for limonene; λ (h^{-1}) is the AER; and β_{SOA} (h^{-1}) is the SOA deposition rate. Using eq 2, we solved for C_{dROG} at each minute with a Runge−Kutta order 4 numerical solution (discussed further below). However, to account for the additional source of C_{dROG} by OH and limonene reactions, we replaced the source term of $kC_{O3}C_{lim}$ (i.e., for ROG ozonolysis only) with one determined by actual changes in limonene for each minute. Equation 2 neglects condensation of oxidation products to chamber walls, as it has been estimated as at least an order of

dx.doi.org/10.1021/es5009906 | Environ. Sci. Technol. 2014, 48, 7899−7908

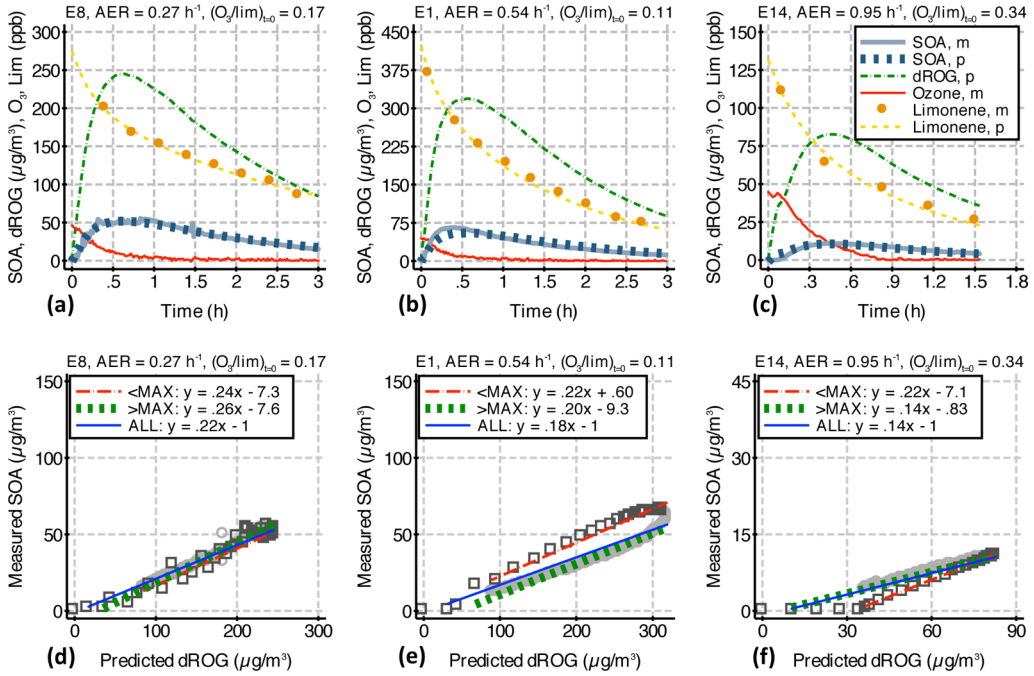

Figure 2. Plots a, b, c: Results for representative transient SOA formation experiments at each of the three air exchange rates (AER) and at low initial ozone–limonene ratios. Measured (m) results for SOA, limonene, and ozone are shown, as well as predicted (p) results for SOA, limonene, and dROG. Plots d, e, f: Linear fits between measured SOA and predicted dROG concentrations using eq 4, for same experiments in plots a, b, and c. Three linear fits are shown: <MAX are fits for SOA > 1 $\mu g/m^3$ and up to the peak SOA concentration; >MAX are for after peak SOA concentration; and ALL are for all SOA with a fixed c^* of 1 $\mu g/m^3$. Hollow dark squares are <MAX, and filled gray circles are >MAX measurements (filled circles appear as a gray band due to close spacing).

magnitude slower than condensation onto aerosols for a chamber at ~1.7 of our chamber surface-to-volume ratio.[64]

Once C_{dROG} is known, if instantaneous equilibrium is assumed, our method describes the time-varying SOA concentration, C_{SOA} ($\mu g/m^3$), with a rearranged form of eq 1:

$$C_{SOA} = C_{dROG}\cdot AMF = C_{dROG}\sum_i \alpha_i\left(1 + \frac{c_i^*}{C_{SOA}}\right)^{-1} \quad (3)$$

Equation 3 thus predicts C_{SOA} as a function of C_{dROG}, and using observed C_{SOA} and calculated C_{dROG}, we can determine the AMF parameters α_i and c_i^* for each experiment. Partitioning for the typical sizes of SOA particles should occur quickly,[65] so the equilibrium assumption is reasonable. One- and two-product solutions have been solved for C_{SOA} with eq 3 for cases without and with background organic aerosol.[63] For our experiments, we found that C_{SOA} was well-described by solving eq 3 with one volatility bin (c^*) without background aerosol, so that the multiproduct solution of eq 3 simplified to this one-product solution:

$$C_{SOA} = C_{dROG}\cdot\alpha\left(1 + \frac{c^*}{C_{SOA}}\right)^{-1} = \alpha C_{dROG} - c^* \quad (4)$$

Therefore, two parameters in eq 4 describe the formation, α and c^*, and with these, C_{SOA} can be algebraically solved for any point in time that C_{dROG} is known. Once the parameters α and c^* are known, the AMF for a particular value of C_{SOA} is determined with eq 1.

Equation 2 for C_{dROG} represents a surrogate for all limonene oxidation products in the SOA or volatile phases and has losses beyond air exchange of (β_{SOA} + [1/AMF]·[d(AMF)/dt]). The reasons for this loss are discussed explicitly in our article[57] with the derivation. However, we should point out two ramifications of this loss term for our method of determining AMF parameters. The first is that the surface loss rate, β_{SOA}, has been included in the C_{dROG} term, so C_{SOA} is not corrected for wall losses directly. In our previous work,[57] we demonstrated that this method produced the same solution as solving for C_{SOA} directly with a differential equation including β_{SOA} (method SOA-M1 in that article). The second is that when solving eq 2, the value of [1/AMF]·[d(AMF)/dt] is required, which is problematic since the AMF parameters are ultimately what are being determined. As such, we solved eq 2 iteratively by determining the AMF at each time step with measured C_{SOA} values and assuming a fixed c^* = 1 $\mu g/m^3$ (see below) while letting α vary for each iteration, until previous and current solutions converged.

RESULTS AND DISCUSSION

Summary of Results. Table 1 lists the experimental conditions, including initial reactant concentrations, as well as results of the peak SOA mass and number size distributions, grouped by the AER with ozone-limited experiments listed first within each group, and the SOA surface deposition rates. Mean (±standard deviation, S.D.) AERs by group were 0.28 (0.02), 0.53 (0.005), and 0.96 (0.008) h^{-1}. The temperature was stable at a mean of 23 °C and RH was less than 10% for all experiments except for E8, during which both were higher due to more extreme laboratory conditions. Across experiments, the measured initial ozone ranged from 45 to 300 ppb and the predicted initial limonene from 20 to 663 ppb.

We can qualitatively compare results across AERs since the initial concentrations for each set of AER experiments were somewhat similar. The maximum SOA mass concentration decreased as the AER increased, and the means (±S.D.) of low,

dx.doi.org/10.1021/es5009906 | Environ. Sci. Technol. 2014, 48, 7899–7908

Table 2. Fits between Measured SOA and Predicted dROG Concentrations, for Three Different Fitting Conditions (See Notes below), Using the Linear One-Product Model in eq 4

	until max SOA[a]			after max SOA[b]			all SOA,[c] fixed c^* = 1 $\mu g/m^3$		
expt. ID[d]	α(<MAX) (−)	c^*(<MAX) ($\mu g/m^3$)	R^2	α(>MAX) (−)	c^*(>MAX) ($\mu g/m^3$)	R^2	α(ALL) (−)	c^*(ALL) ($\mu g/m^3$)	R^2
moderate air exchange rate experiments									
E1	0.22	−0.63	0.98	0.20	9.3	0.96	0.18	1	0.85
E2	0.34	−0.38	0.99	0.33	0.9	1.00	0.34	1	0.99
E3	0.24	−0.44	0.99	0.25	1.3	1.00	0.25	1	0.96
E4[e]	0.88	3.5	0.99	0.79	0.85	1.00	0.80	1	0.99
E5[e]	0.62	7.4	1.00	0.51	1.1	1.00	0.51	1	0.99
E6	0.37	0.26	0.99	0.36	1.5	1.00	0.36	1	0.97
low air exchange rate experiments									
E7	0.18	−5.0	0.67	0.25	8.2	0.99	0.21	1	0.90
E8	0.24	7.3	0.93	0.26	7.6	0.98	0.22	1	0.95
E9	0.39	5.3	0.96	0.32	−3.0	0.97	0.36	1	0.95
E10	0.54	77	0.96	0.41	−38	1.00	0.46	1	0.88
E11	0.50	−0.92	0.97	0.52	7.5	0.98	0.49	1	0.90
E12	0.31	1.3	0.94	0.33	10	0.98	0.29	1	0.94
high air exchange rate experiments									
E13	0.042	4.2	0.95	0.030	2.7	0.94	0.027	1	0.70
E14	0.22	7.1	1.00	0.14	0.83	0.99	0.14	1	0.97
E15	0.21	3.2	1.00	0.13	−0.040	0.99	0.15	1	0.85
E16	0.38	13	0.99	0.28	3.7	0.99	0.26	1	0.95
E17[e]	0.42	5.3	1.00	0.37	2.3	0.99	0.34	1	0.91
E18	0.29	0.66	0.99	0.26	0.011	1.00	0.29	1	0.95

[a]<MAX fits for are fits for SOA > 1 $\mu g/m^3$ and up to the peak SOA concentration. [b]>MAX fits for after peak SOA concentration. [c]ALL fits for all SOA with a fixed c^* = 1 $\mu g/m^3$. [d]Experiment identification number. [e]Experiments of E4, E5, and E17 had poor agreement between measured and modeled limonene and are not included in further analysis (see text for details).

moderate, and high AERs were 109 (107), 37 (18), and 17 (12) $\mu g/m^3$, respectively. Peak number was also negatively related to AER, and the mean numbers (±S.D.) at low, moderate, and high AERs were 2.23×10^5 (1.60×10^5), 1.89×10^5 (9.15×10^4), and 9.53×10^4 (8.86×10^4) #/cm^3, respectively. The peak size distributions were log-normal, but their geometric means (GM) and geometric standard deviation (GSD) were not functions of the AER; the mean GMs for the three AERs ranged from 40 to 59 nm, and GSDs of ∼1.5 were constant over nearly all experiments. Overall, peak GMs were lower than those in Waring et al.[13] for a semibatch system, but GSDs were similar. Peak number always occurred earlier than peak mass.

Transient SOA Formation. Figure 2a−c illustrates time-resolved results for three experiments, with one at each AER for low initial ozone−limonene ratios. (Note the differences in scale for the ordinates in this plot. These plots are not meant to convey a representative decrease in SOA formed due to AER changes; this and other relationships are quantified in later analyses.) Measured ozone, limonene, and SOA are shown, along with predicted limonene, C_{dROG}, and C_{SOA} (SOA prediction discussed below). At t = 0 h, the ozone and limonene began decaying from chemical reactions and air exchange. As ozone and limonene reacted, the SOA increased, peaked, and then decreased due to air exchange and deposition, as well as because the SOA formation strength decreased as the ozone and limonene decreased. The C_{dROG} behaved similarly in trend to C_{SOA}. Most experiments showed good agreement between the measured and predicted limonene, with agreement slopes of 0.95−1.02 and $R^2 \geq 0.81$. However, E4 and E5 had poor fits, and E17 was fit with only one data point, so the results from these experiments are not included in analysis in the Parameterizing Transient SOA Formation and Implications for Indoor SOA Formation sections.

To assess the influence of OH−limonene conversion, we compared the results of peak C_{dROG} across experiments when predicting C_{dROG} with (*i*) the source term using observed changes in limonene (which was what we used to generate C_{dROG} for our analysis) and with (*ii*) the source term of $kC_{O3}C_{lim}$ (k = 0.0183 ppb^{-1} h^{-1})[62] assuming that their difference was from OH−limonene oxidation. This analysis suggested that an average of 91% of limonene reacted with ozone and 9% with OH. Our experiments used methanol as a solvent to introduce the limonene. Using an OH modeling approach similar to Chen and Hopke[55] but including estimated methanol as well, we predict that if methanol were not present that 73% of limonene would have reacted with ozone and 27% with OH. However, OH reactions with limonene yield products with three added oxygen atoms[66] that are similar to ozonolysis products, so the product volatility distribution and resulting AMFs should be little affected.[67]

Figure 2d−f show measured C_{SOA} versus predicted C_{dROG} for the same three experiments. For these and all experiments, AMF parameters of α and c^* were fit to the C_{SOA} as a function of C_{dROG} using eq 4. Example linear fits are in Figure 2d−f, and fits for all experiments are in Table 2. We performed three distinct fits to the data: (*i*) the first "<MAX" is a fit for results prior to the peak SOA concentration and once the new C_{SOA} exceeded 1 $\mu g/m^3$; (*ii*) the second ">MAX" is for results after the peak SOA concentration; and (*iii*) the third "ALL" is for all SOA results but with a fixed c^* = 1 $\mu g/m^3$. The overall uncertainties for these parameters are less than 15%, given measurement uncertainties. The ALL fit was assigned c^* = 1 $\mu g/m^3$ since the average c^* for <MAX and >MAX fits was 1.95 $\mu g/m^3$ (if E10 for <MAX is excluded). Since it well represents the entire experimental duration, the ALL fit is useful to predict C_{SOA} by using C_{dROG} with its α and c^* = 1 $\mu g/m^3$ within eq 4,

dx.doi.org/10.1021/es5009906 | Environ. Sci. Technol. 2014, 48, 7899−7908

which is how the predicted C_{SOA}'s were determined for Figure 2a–c. Additionally, as stated in the Methodology, this ALL α fit was used to determine the AMF for eq 2 when solving for C_{dROG} iteratively.

The <MAX fits describe the formation from the initial combination of the reactants until the peak SOA concentration, and they have on average slightly higher α (i.e., steeper slopes) than the >MAX or ALL fits. On average for all considered experiments, the higher α corresponds to the larger c^* (i.e., more negative y intercepts) for the <MAX periods versus the >MAX or ALL periods. This trend of larger average c^* for <MAX periods arises because some amount of limonene must be converted before a sufficient amount of C_{dROG} is generated to begin forming SOA mass. Correspondingly, in Figure 2d–f, the hollow dark squares for the results during the <MAX period demonstrate that some threshold value for C_{dROG} was always reached before C_{SOA} began forming. For the oxidation of different ROGs that generates a distribution of products with a higher volatility than limonene ozonolysis, this effect would be even more pronounced.

Parameterizing Transient SOA Formation. Using the ALL fitted results with eq 1, Figure 3 displays AMFs as a function of the maximum C_{SOA} concentration for each experiment, as well as individual AMFs from batch experiments at similar temperatures and ozone–limonene ratios from Leungsakul et al.[40] To interpret these AMFs within the realm of limonene ozonolysis SOA formation potential, we plotted the dark limonene ozonolysis AMF fit from Zhang et al.,[47] which is an upper bound and represents fully oxidized limonene, and the dark limona ketone ozonolysis AMF fit from Donahue et al.,[49] which is a lower bound and represents only endo- bond oxidized limonene. All but one of our AMFs and those from Leungsakul et al.[40] reside within this SOA formation potential space. We chose not to fit an AMF curve to our results because they do not represent a specific reaction regime (i.e., both endo/exo- bond oxidation or endo- bond oxidation only), and a fit would thus have little meaning.

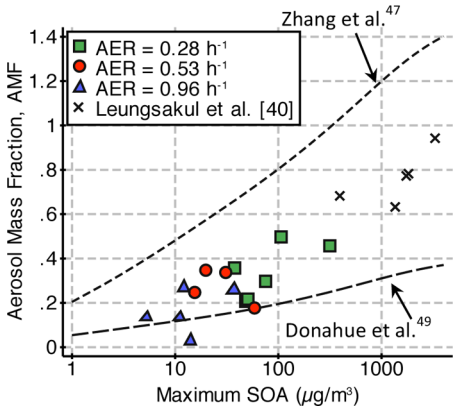

Figure 3. Aerosol mass fraction as a function of maximum SOA concentration assuming the one-product model using α(ALL) for c^* = 1 μg/m^3 for our experiments, as well as results from batch AMFs from Leungsakul et al.[40] at similar temperatures. Also shown are volatility basis set curve fits for AMFs for results from Zhang et al.[47] for dark limonene ozonolysis and from Donahue et al.[49] for dark limona ketone ozonolysis.

The AMFs fluctuate within that space because of variations in ozone–limonene ratios or AERs. As stated earlier, increases in ozone–limonene ratios increase the secondary reaction rate of ozone attack on the exo- bond in the aerosol phase (at low NO_x),[47,50] and increases in AERs reduce time for those later generation reactions to occur. The time scales of these two mechanisms thus compete to affect formation. To explore this, Figure 4 shows the AMF as a function of the ratio of the lifetime for heterogeneous ozone reactions with first-generation ozonolysis products in the aerosol phase and the chamber residence time (i.e., inverse of AER). The ozone heterogeneous lifetime was calculated at each maximum C_{SOA}, using the procedure in Zhang et al.[47] and assuming an ozone uptake coefficient of γ = 0.001. Clearly, the interplay of these two mechanisms affects the AMF, with what appears to be a strong dependence of the AMF on the ability of ozone having sufficient time to oxidize the exo- limonene double bond.

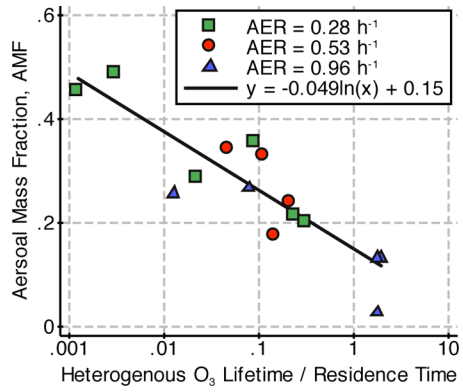

Figure 4. Aerosol mass fraction, assuming the one-product model using α(ALL) for c^* = 1 μg/m^3, as a function of ratio of heterogeneous lifetime for ozone reacting with first-generation products in the SOA phase and chamber residence time (i.e., inverse of air exchange rate, AER). The ozone heterogeneous lifetime was calculated using the procedure in Zhang et al.[47] and assuming an ozone uptake coefficient of γ = 0.001. The R^2 = 0.73 for the natural log fit to the data.

Using this insight as guidance, we conducted multiple linear regressions for the fits in Table 2. The outcomes were the AMF parameters (α and c^*), and predictors were the (*i*) product of initial ozone and limonene concentrations, (*ii*) AER, and (*iii*) initial ozone–limonene ratio, as shown in eq 5:

$$\alpha,\ c^* = \beta_0 + \beta_1(C_{O3}C_{lim})_{t=0} + \beta_2\lambda + \beta_3\left(\frac{C_{O3}}{C_{lim}}\right)_{t=0} \quad (5)$$

where β_n are regression coefficients for each input variable n. AMFs from Leungsakul et al.[40] were also included, since those were from similar ozone–limonene ratios but in a batch system (AER $\approx$ 0.01 h^{-1}). Regression coefficients are in Table 3, along with p values (bolded if significance <0.05), standardized regression coefficients (SRC), and R^2 values. SRCs can be used to compare the relative impacts of inputs on the outcome and are the actual regression coefficients normalized by the ratio of the sample standard deviations of the dependent to independent variables. SRCs range from −1 to +1 (unless predictor variables exhibit multicollinearity); a high |SRC| indicates a large influence on the outcome, while a |SRC| near zero indicates little influence, and an input with a −SRC changes the outcome negatively and a +SRC changes the outcome positively.[68]

According to the regressions, the α(<MAX), α(>MAX), and α(ALL) parameters are affected by the AER negatively and initial ozone–limonene ratio positively, in accordance with our

dx.doi.org/10.1021/es5009906 | Environ. Sci. Technol. 2014, 48, 7899–7908

Table 3. Multiple Linear Regression Fits for Outcome Variables of α and c^* Listed in Table 2 with Input Variables of the Initial Ozone-Limonene Product, Air Exchange Rate, and Initial Ozone-Limonene Ratio for Each Experiment[a]

outcome	statistic[b]	$(C_{O3}C_{lim})_{t=0}$[c]	AER[d]	$(C_{O3}/C_{lim})_{t=0}$[e]	y intercept	R^2
α(<MAX)	Coef.	1.4×10^{-06}	**−0.24**	**0.061**	**0.35**	0.67
	p-value	0.31	**0.010**	**0.0034**	**7.8×10^{-05}**	
	SRC	0.19	**−0.58**	**0.67**		
c^*(<MAX)	Coef.	**0.0010**	1.9	1.3	−10	0.81
	p-value	**3.58×10^{-05}**	0.84	0.50	0.15	
	SRC	**0.90**	0.029	0.095		
α(>MAX)	Coef.	-3.1×10^{-07}	**−0.33**	**0.055**	**0.40**	0.82
	p-value	0.74	**9.0×10^{-05}**	**0.00051**	**6.2×10^{-07}**	
	SRC	−0.046	**−0.84**	**0.65**		
c^*(>MAX)	Coef.	**−0.00052**	−3.9	−0.077	11	0.60
	p-value	**0.0020**	0.63	0.96	0.078	
	SRC	**−0.80**	−0.10	−0.0095		
α(ALL)	Coef.	**8.3×10^{-07}**	**−0.46**	**0.053**	**0.48**	0.83
	p-value	**0.0035**	**6.7×10^{-05}**	**0.029**	**6.4×10^{-08}**	
	SRC	**0.41**	**−0.67**	**0.26**		

[a]Bolded values are significant in the regression. [b]Coef. = regression coefficient; p-value < 0.05 indicates significance of the input or intercept in the regression; SRC = standardized regression coefficient. [c]$(C_{O3}C_{lim})_{t=0}$ = initial ozone−limonene product in the experiment. [d]AER = air exchange rate in the experiment. [e]$(C_{O3}/C_{lim})_{t=0}$ = initial ozone−limonene ratio in the experiment.

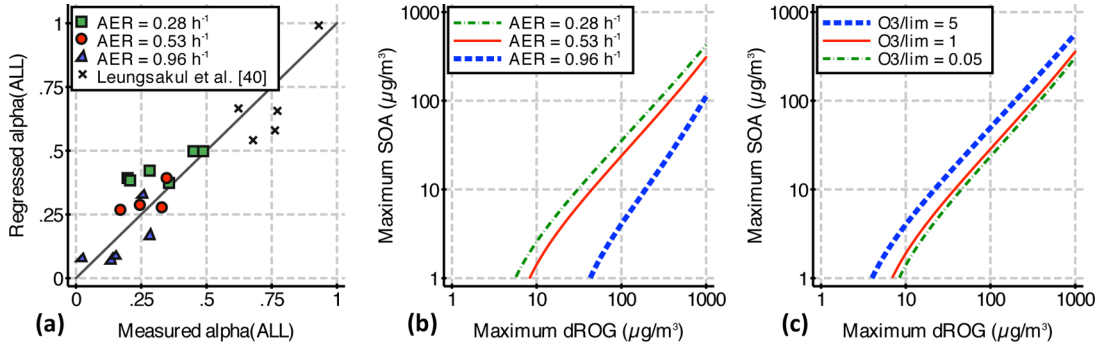

Figure 5. (a) Regressed α(ALL) versus the measured α(ALL) (i.e., $c^* = 1$ $\mu g/m^3$), using regression coefficients in Table 3 ($R^2 = 0.83$), along with a 1:1 line. Using that regression, the other plots show the prediction of (b) maximum SOA as a function of the maximum dROG for air exchange rates (AER) of 0.28, 0.53, and 0.96 h^{-1}, with an initial ozone−limonene ratio of 0.1, and (c) maximum SOA as a function of maximum dROG for ozone−limonene ratios of 0.05, 1, and 5, with an AER of 0.53 h^{-1}.

time scale analysis. The c^*(<MAX) is positively affected and the c^*(>MAX) is negatively affected by the initial ozone−limonene product, because higher ROG conversion leads to more volatile products comprising the SOA.[47,48,67] More volatile products can condense at higher C_{SOA}, increasing c^*(<MAX), and are more affected by differing loss rates of SOA and volatile products as both decrease in the chamber, decreasing c^*(>MAX). Finally, the positive influence of α(ALL) with the initial ozone−limonene product indicates that stronger formation occurs at the increased SOA loading that follows from higher rates of ROG conversion. According to SRCs for the α(ALL) regression, the AER has the strongest influence on SOA formation potential, followed by the ozone−limonene product and then the ozone−limonene ratio.

Implications for Indoor SOA Formation. Transient α(ALL) AMF parameters were used to explore the maximum C_{SOA} formed as a function of maximum C_{dROG} of 1 to 1000 $\mu g/m^3$ over AER and initial ozone−limonene conditions. For these simple examples, we estimated that the maximum $C_{dROG} = 83.2$ times the initial ozone−limonene product, as determined from our experimental data. For each maximum C_{dROG}, we used the α(ALL) regression coefficients in eq 5 to estimate the α, and then we used that α to predict the maximum C_{SOA} formed with eq 4. Figure 5a illustrates good agreement between predicted and measured α(ALL) values. Figure 5b shows the maximum C_{SOA} as a function of maximum C_{dROG} for our AERs of 0.28, 0.53, and 0.96 h^{-1}, for an ozone−limonene ratio of 0.1, which is a reasonable value for limonene pulse emissions in the presence of indoor ozone mole fractions.[18,21] In Figure 5c, we display formation for different ozone−limonene ratios of 0.05, 1, and 5, which cover the range in this work, for an AER of 0.53 h^{-1}, the median for U.S. residences.[51]

Figure 5b,c graphically demonstrates that increases in AERs and decreases in ozone−limonene ratios require more C_{dROG} to generate equivalent values of C_{SOA} for indoor environments. The effects of the studied variables (i.e., AER, initial ozone−limonene ratio and product) have larger impacts on SOA formation at lower C_{dROG}. Also, Figure 5b and c illustrate that the AER affects the formation more than the ozone−limonene ratio, as suggested by the SRCs. Increasing the AER from 0.53 to 0.96 h^{-1} decreases SOA relatively more than increasing from 0.28 to 0.53 h^{-1}, implying that when predicting formation in spaces with high AERs, it is especially important to consider the AMF relationships quantified in this work. When ozone−limonene ratios are <1, the AMF is less influenced than when

dx.doi.org/10.1021/es5009906 | Environ. Sci. Technol. 2014, 48, 7899−7908

the ratio > 1, which is expected since when the ratio > 1, exo-bond oxidation occurs.

AMF parameters in this work can be reproduced with our regression coefficients over our studied range of conditions, and they can be used to predict indoor SOA formation due to ozonolysis of pulse-emitted limonene. This study highlights the importance of quantifying indoor SOA formation with AMFs from experiments performed in chambers with air exchange and at initial ozone−limonene concentrations typical of indoors. Regarding limonene ozonolysis, AMFs determined in batch chambers with high ozone−limonene ratios (e.g., Zhang et al.[47]) may be inappropriate for indoor SOA formation prediction for certain circumstances. We reiterate that this work was conducted at low RH and without background aerosol, and these conditions influenced our results. Jonsson et al.[69] showed that increases in RH from ∼2 to 85% can impact SOA mass growth by large factors of 4−8 in a laminar plug flow reaction system. Background organic aerosol can easily be included in our framework by solving eq 3 for an initial amount of organic aerosol present.[57,63] Finally, we are conducting similar experiments with other indoor terpenoids, such as α-pinene and α-terpineol. However, AMFs for these terpenoids will likely not exhibit the same dependence as limonene on the AER or initial concentrations, since these terpenoids only have one double bond and secondary ozone reactions are nonexistent.

AUTHOR INFORMATION

Corresponding Author

*Telephone: 1-215-895-1502. Fax: 1-215-895-1363. E-mail: msw59@drexel.edu.

Notes

The authors declare no competing financial interest.

ACKNOWLEDGMENTS

This work was funded by the National Science Foundation (Award #1055584). We also thank the efforts of the reviewers, whose suggestions improved this manuscript.

REFERENCES

(1) Abdullahi, K. L.; Delgado-Saborit, J. M.; Harrison, R. M. Emissions and indoor concentrations of particulate matter and its specific chemical components from cooking: A review. *Atmos. Environ.* **2013**, *71*, 260−294, DOI: 10.1016/j.atmosenv.2013.01.061.

(2) Lai, A. C. K. Modeling of airborne particle exposure and effectiveness of engineering control strategies. *Build. Environ.* **2004**, *39* (6), 599−610, DOI: 10.1016/j.buildenv.2003.12.005.

(3) Luoma, M.; Batterman, S. A. Characterization of Particulate Emissions from Occupant Activities in Offices. *Indoor Air* **2001**, *11* (1), 35−48, DOI: 10.1034/j.1600-0668.2001.011001035.x.

(4) Morawska, L.; Afshari, A.; Bae, G. N.; Buonanno, G.; Chao, C. Y. H.; Hänninen, O.; Hofmann, W.; Isaxon, C.; Jayaratne, E. R.; Pasanen, P.; Salthammer, T.; Waring, M.; Wierzbicka, A. Indoor aerosols: from personal exposure to risk assessment. *Indoor Air* **2013**, *23* (6), 462−487, DOI: 10.1111/ina.12044.

(5) Presto, A. A.; Miracolo, M. A.; Kroll, J. H.; Worsnop, D. R.; Robinson, A. L.; Donahue, N. M. Intermediate-volatility organic compounds: A potential source of ambient oxidized organic aerosol. *Environ. Sci. Technol.* **2009**, *43* (13), 4744−4749, DOI: 10.1021/es803219q.

(6) Turpin, B. J.; Huntzicker, J. J. Identification of secondary organic aerosol episodes and quantitation of primary and secondary organic aerosol concentrations during SCAQS. *Atmos. Environ.* **1995**, *29* (23), 3527−3527, DOI: 10.1016/1352-2310(94)00276-Q.

(7) Chen, X.; Hopke, P. K. In *A Chamber Study of Secondary Organic Aerosol Formation from Ozonolysis of -Pinene and Linalool*; 9th International Healthy Buildings Conference and Exhibition, HB 2009, September 13−17, 2009, Syracuse, NY, United States; International Society of Indoor Air Quality and Climate: Syracuse, NY, 2009.

(8) Weschler, C. J.; Shields, H. C. Indoor ozone/terpene reactions as a source of indoor particles. *Atmos. Environ.* **1999**, *33* (15), 2301−2312, http://dx.doi.org/10.1016/S1352-2310(99)00083-7.

(9) Sarwar, G.; Corsi, R.; Allen, D.; Weschler, C. The significance of secondary organic aerosol formation and growth in buildings: experimental and computational evidence. *Atmos. Environ.* **2003**, *37* (9−10), 1365−1381, http://dx.doi.org/10.1016/S1352-2310(02)01013-0.

(10) Chen, X.; Hopke, P. K. Secondary organic aerosol from α-pinene ozonolysis in dynamic chamber system. *Indoor Air* **2009**, *19* (4), 335−345, DOI: 10.1111/j.1600-0668.2009.00596.x.

(11) Zuraimi, M. S.; Weschler, C. J.; Tham, K. W.; Fadeyi, M. O. The impact of building recirculation rates on secondary organic aerosols generated by indoor chemistry. *Atmos. Environ.* **2007**, *41* (25), 5213−5223, http://dx.doi.org/10.1016/j.atmosenv.2006.05.087.

(12) Grosjean, D.; Seinfeld, J. H. Parameterization of the formation potential of secondary organic aerosols. *Atmos. Environ.* **1989**, *23* (8), 1733−1747, DOI: 10.1016/0004-6981(89)90058-9.

(13) Waring, M. S.; Wells, J. R.; Siegel, J. A. Secondary organic aerosol formation from ozone reactions with single terpenoids and terpenoid mixtures. *Atmos. Environ.* **2011**, *45* (25), 4235−4242, DOI: 10.1016/j.atmosenv.2011.05.001.

(14) Sarwar, G.; Corsi, R. The effects of ozone/limonene reactions on indoor secondary organic aerosols. *Atmos. Environ.* **2007**, *41* (5), 959−973, DOI: 10.1016/j.atmosenv.2006.09.032.

(15) Sarwar, G.; Olson, D. A.; Corsi, R. L.; Weschler, C. J. Indoor Fine Particles: The Role of Terpene Emissions from Consumer Products. *J. Air Waste Manage. Assoc.* **2004**, *54* (3), 367−377, DOI: 10.1080/10473289.2004.10470910.

(16) Waring, M. S. Secondary organic aerosol in residences: predicting its fraction of fine particle mass and determinants of formation strength. *Indoor Air* **2014**, DOI: 10.1111/ina.12092.

(17) Sabersky, R. H.; Sinema, D. A.; Shair, F. H. Concentrations, decay rates, and removal of ozone and their relation to establishing clean indoor air. *Environ. Sci. Technol.* **1973**, *7* (4), 347−353, DOI: 10.1021/es60076a001.

(18) Weschler, C. J. Ozone in Indoor Environments: Concentration and Chemistry. *Indoor Air* **2000**, *10* (4), 269−288, DOI: 10.1034/j.1600-0668.2000.010004269.x.

(19) Waring, M. S.; Siegel, J. A.; Corsi, R. L. Ultrafine particle removal and generation by portable air cleaners. *Atmos. Environ.* **2008**, *42* (20), 5003−5014, http://dx.doi.org/10.1016/j.atmosenv.2008.02.011.

(20) Lee, S. C.; Lam, S.; Kin Fai, H. Characterization of VOCs, ozone, and PM10 emissions from office equipment in an environmental chamber. *Build. Environ.* **2001**, *36* (7), 837−842, DOI: 10.1016/s0360-1323(01)00009-9.

(21) Singer, B. C.; Coleman, B. K.; Destaillats, H.; Hodgson, A. T.; Lunden, M. M.; Weschler, C. J.; Nazaroff, W. W. Indoor secondary pollutants from cleaning product and air freshener use in the presence of ozone. *Atmos. Environ.* **2006**, *40* (35), 6696−6710, http://dx.doi.org/10.1016/j.atmosenv.2006.06.005.

(22) Nazaroff, W. W.; Weschler, C. J. Cleaning products and air fresheners: exposure to primary and secondary air pollutants. *Atmos. Environ.* **2004**, *38* (18), 2841−2865, http://dx.doi.org/10.1016/j.atmosenv.2004.02.040.

(23) Weisel, C. P.; Zhang, J.; Turpin, B. J.; Morandi, M. T.; Colome, S.; Stock, T. H.; Spektor, D. M. Relationships of Indoor, Outdoor, and Personal Air (RIOPA) Part I. Collection Methods and Descriptive Analyses. *Res. Rep. Health Eff. Inst.* **2005**, *Nov*, 109−127.

(24) Donahue, N. M.; Huff Hartz, K. E.; Bao, C.; Presto, A. A.; Stanier, C. O.; Rosenhorn, T.; Robinson, A. L.; Pandis, S. N. Critical factors determining the variation in SOA yields from terpene

ozonolysis: a combined experimental and computational study. *Faraday Discuss.* **2005**, *130*, 295−309, DOI: 10.1039/b417369d.
(25) Kroll, J. H.; Chan, A. W. H.; Ng, N. L.; Flagan, R. C.; Seinfeld, J. H. Reactions of semivolatile organics and their effects on secondary organic aerosol formation. *Environ. Sci. Technol.* **2007**, *41* (10), 3545−3550, DOI: 10.1021/es062059x.
(26) Lim, Y. B.; Ziemann, P. J. Effects of molecular structure on aerosol yields from OH radical-initiated reactions of linear, branched, and cyclic alkanes in the presence of NOx. *Environ. Sci. Technol.* **2009**, *43* (7), 2328−34, DOI: 10.1021/es803389s.
(27) Miracolo, M. A.; Presto, A. A.; Lambe, A. T.; Hennigan, C. J.; Donahue, N. M.; Kroll, J. H.; Worsnop, D. R.; Robinson, A. L. Photo-oxidation of low-volatility organics found in motor vehicle emissions: Production and chemical evolution of organic aerosol mass. *Environ. Sci. Technol.* **2010**, *44* (5), 1638−1643, DOI: 10.1021/es902635c.
(28) Presto, A. A.; Miracolo, M. A.; Donahue, N. M.; Robinson, A. L. Secondary organic aerosol formation from high-NOx Photo-oxidation of low volatility precursors: N-alkanes. *Environ. Sci. Technol.* **2010**, *44* (6), 2029−2034, DOI: 10.1021/es903712r.
(29) Chan, A. W. H.; Kautzman, K. E.; Chhabra, P. S.; Surratt, J. D.; Chan, M. N.; Crounse, J. D.; Kürten, A.; Wennberg, P. O.; Flagan, R. C.; Seinfeld, J. H. Secondary organic aerosol formation from photooxidation of naphthalene and alkylnaphthalenes: implications for oxidation of intermediate volatility organic compounds (IVOCs). *Atmos. Chem. Phys.* **2009**, *9* (9), DOI: 10.5194/acp-9-3049-2009.
(30) Pandis, S. N.; Harley, R. A.; Cass, G. R.; Seinfeld, J. H. Secondary organic aerosol formation and transport. *Atmos. Environ., Part A* **1992**, *26 A* (13), 2269−2282, http://dx.doi.org/10.1016/0960-1686(92)90358-R.
(31) Pandis, S. N.; Wexler, A. S.; Seinfeld, J. H. Secondary organic aerosol formation and transport-II. Predicting the ambient secondary organic aerosol size distribution. *Atmos. Environ., Part A* **1993**, *27 A* (15), 2403−2416, DOI: 10.1016/0960-1686(93)90408-Q.
(32) Odum, J. R.; Hoffmann, T.; Bowman, F.; Collins, D.; Flagan, R. C.; Seinfeld, J. H. Gas/particle partitioning and secondary organic aerosol yields. *Environ. Sci. Technol.* **1996**, *30* (8), 2580−2585, DOI: 10.1021/es950943+.
(33) Pankow, J. F. An absorption model of gas/particle partitioning of organic compounds in the atmosphere. *Atmos. Environ.* **1994**, *28* (2), 185−188, http://dx.doi.org/10.1016/1352-2310(94)90093-0.
(34) Pankow, J. F. An absorption model of the gas/aerosol partitioning involved in the formation of secondary organic aerosol. *Atmos. Environ.* **1994**, *28* (2), 189−193, http://dx.doi.org/10.1016/1352-2310(94)90094-9.
(35) Hoffmann, T.; Odum, J. R.; Bowman, F.; Collins, D. Formation of Organic Aerosols from the Oxidation of Biogenic Hydrocarbons. *J. Atmos. Chem.* **1997**, *26* (2), 189−189, DOI: 10.1023/A:1005734301837.
(36) Griffin, R. J.; Cocker, D. R., III; Flagan, R. C.; Seinfeld, J. H. Organic aerosol formation from the oxidation of biogenic hydrocarbons. *J. Geophys. Res.* **1999**, *104* (D3), 3555−67, DOI: 10.1029/1998JD100049.
(37) Cocker Iii, D. R.; Clegg, S. L.; Flagan, R. C.; Seinfeld, J. H. The effect of water on gas-particle partitioning of secondary organic aerosol. Part I: -pinene/ozone system. *Atmos. Environ.* **2001**, *35* (35), 6049−6072, DOI: 10.1016/S1352-2310(01)00404-6.
(38) Ng, N. L.; Kroll, J. H.; Keywood, M. D.; Bahreini, R.; Varutbangkul, V.; Flagan, R. C.; Seinfeld, J. H.; Lee, A.; Goldstein, A. H. Contribution of first- versus second-generation products to secondary organic aerosols formed in the oxidation of biogenic hydrocarbons. *Environ. Sci. Technol.* **2006**, *40* (7), 2283−2297, DOI: 10.1021/es052269u.
(39) Dommen, J.; Metzger, A.; Duplissy, J.; Kalberer, M.; Alfarra, M. R.; Gascho, A.; Weingartner, E.; Prevot, A. S. H.; Verheggen, B.; Baltensperger, U. Laboratory observation of oligomers in the aerosol from isoprene/NO x photooxidation. *Geophys. Res. Lett.* **2006**, *33* (13), DOI: 10.1029/2006GL026523.
(40) Leungsakul, S.; Jaoui, M.; Kamens, R. M. Kinetic mechanism for predicting secondary organic aerosol formation from the reaction of d-limonene with ozone. *Environ. Sci. Technol.* **2005**, *39* (24), 9583−9594, DOI: 10.1021/es0492687.
(41) Leungsakul, S.; Jeffries, H. E.; Kamens, R. M. A kinetic mechanism for predicting secondary aerosol formation from the reactions of d-limonene in the presence of oxides of nitrogen and natural sunlight. *Atmos. Environ.* **2005**, *39* (37), 7063−7082, DOI: 10.1016/j.atmosenv.2005.08.024.
(42) Kroll, J. H.; Ng, N. L.; Murphy, S. M.; Flagan, R. C.; Seinfeld, J. H. Secondary organic aerosol formation from isoprene photooxidation. *Environ. Sci. Technol.* **2006**, *40* (6), 1869−1877, DOI: 10.1021/es0524301.
(43) Zhou, Y.; Zhang, H.; Parikh, H. M.; Chen, E. H.; Rattanavaraha, W.; Rosen, E. P.; Wang, W.; Kamens, R. M. Secondary organic aerosol formation from xylenes and mixtures of toluene and xylenes in an atmospheric urban hydrocarbon mixture: Water and particle seed effects (II). *Atmos. Environ.* **2011**, *45* (23), 3882−3890, DOI: 10.1016/j.atmosenv.2010.12.048.
(44) Liu, C.; Chu, B.; Liu, Y.; Ma, Q.; Ma, J.; He, H.; Li, J.; Hao, J. Effect of mineral dust on secondary organic aerosol yield and aerosol size in -pinene/NOx photo-oxidation. *Atmos. Environ.* **2013**, *77*, 781−789, DOI: 10.1016/j.atmosenv.2013.05.064.
(45) Hatfield, M. L.; Huff Hartz, K. E. Secondary organic aerosol from biogenic volatile organic compound mixtures. *Atmos. Environ.* **2011**, *45* (13), 2211−2219, http://dx.doi.org/10.1016/j.atmosenv.2011.01.065.
(46) Chen, T.; Jang, M. Secondary organic aerosol formation from photooxidation of a mixture of dimethyl sulfide and isoprene. *Atmos. Environ.* **2012**, *46* (0), 271−278, DOI: 10.1016/j.atmosenv.2011.09.082.
(47) Zhang, J.; Huff Hartz, K. E.; Pandis, S. N.; Donahue, N. M. Secondary organic aerosol formation from limonene Ozonolysis: Homogeneous and heterogeneous influences as a function of NOx. *J. Phys. Chem. A* **2006**, *110* (38), 11053−11063, DOI: 10.1021/jp062836f.
(48) Presto, A. A.; Donahue, N. M. Investigation of -pinene + ozone secondary organic aerosol formation at low total aerosol mass. *Environ. Sci. Technol.* **2006**, *40* (11), 3536−3543, DOI: 10.1021/es052203z.
(49) Donahue, N. M.; Tischuk, J. E.; Marquis, B. J.; Huff Hartz, K. E. Secondary organic aerosol from limona ketone: insights into terpene ozonolysis via synthesis of key intermediates. *Phys. Chem. Chem. Phys.* **2007**, *9* (23), 2991−2998, DOI: 10.1039/B701333G.
(50) Maksymiuk, C. S.; Gayahtri, C.; Gil, R. R.; Donahue, N. M. Secondary organic aerosol formation from multiphase oxidation of limonene by ozone: mechanistic constraints via two-dimensional heteronuclear NMR spectroscopy. *Phys. Chem. Chem. Phys.* **2009**, *11* (36), 7810−18, DOI: 10.1039/b820005j.
(51) Murray, D. M.; Burmaster, D. E. Residential air exchange rates in the United States: Empirical and estimated parametric distributions by season and climatic region. *Risk Anal.* **1995**, *15* (4), 459−465, DOI: 10.1111/j.1539-6924.1995.tb00338.x.
(52) EPA Building Assessment Survey and Evaluation (BASE) Study. http://www.epa.gov/iaq/base/.
(53) Fadeyi, M. O.; Weschler, C. J.; Tham, K. W. The impact of recirculation, ventilation and filters on secondary organic aerosols generated by indoor chemistry. *Atmos. Environ.* **2009**, *43* (22−23), 3538−3547, DOI: 10.1016/j.atmosenv.2009.04.017.
(54) Shilling, J. E.; Chen, Q.; King, S. M.; Rosenoern, T.; Kroll, J. H.; Worsnop, D. R.; McKinney, K. A.; Martin, S. T. Particle mass yield in secondary organic aerosol formed by the dark ozonolysis of α-pinene. *Atmos. Chem. Phys.* **2008**, *8* (7), 2073−2088, DOI: 10.5194/acp-8-2073-2008.
(55) Chen, X.; Hopke, P. K. A chamber study of secondary organic aerosol formation by limonene ozonolysis. *Indoor Air* **2010**, *20* (4), 320−328, DOI: 10.1111/j.1600-0668.2010.00656.x.
(56) Destaillats, H.; Lunden, M. M.; Singer, B. C.; Coleman, B. K.; Hodgson, A. T.; Weschler, C. J.; Nazaroff, W. W. Indoor Secondary Pollutants from Household Product Emissions in the Presence of Ozone: A Bench-Scale Chamber Study. *Environ. Sci. Technol.* **2006**, *40* (14), 4421−4428, DOI: 10.1021/es052198z.

(57) Youssefi, S.; Waring, M. S. Predicting secondary organic aerosol formation from terpenoid ozonolysis with varying yields in indoor environments. *Indoor Air* **2012**, *22* (5), 415−426, DOI: 10.1111/j.1600-0668.2012.00776.x.
(58) Atkinson, R.; Aschmann, S. M. Hydroxyl radical production from the gas-phase reactions of ozone with a series of alkenes under atmospheric conditions. *Environ. Sci. Technol.* **1993**, *27* (7), 1357−1363, DOI: 10.1021/es00044a010.
(59) Atkinson, R.; Aschmann, S. M.; Arey, J.; Shorees, B. Formation of OH radicals in the gas phase reactions of O3 with a series of terpenes. *J. Geophys. Res.: Atmos.* **1992**, *97* (D5), 6065−6073, DOI: 10.1029/92JD00062.
(60) Anglada, J. M.; Aplincourt, P.; Bofill, J. M.; Cremer, D. Atmospheric Formation of OH Radicals and H2O2 from Alkene Ozonolysis under Humid Conditions. *ChemPhysChem* **2002**, *3* (2), 215−221, DOI: 10.1002/1439-7641(20020215)3:2<215::AID-CPHC215>3.0.CO;2-3.
(61) Aschmann, S. M.; Arey, J.; Atkinson, R. OH radical formation from the gas-phase reactions of O3 with a series of terpenes. *Atmos. Environ.* **2002**, *36* (27), 4347−4355, DOI: 10.1016/S1352-2310(02)00355-2.
(62) Atkinson, R.; Hasegawa, D.; Aschmann, S. M. Rate Constants for the Gas-Phase Reactions of O-3 with a Series of Monoterpenes and Related-Compounds at 296-K ±2-K. *Int. J. Chem. Kinet.* **1990**, *22* (8), 871−887, DOI: 10.1002/kin.550220807.
(63) Kroll, J. H.; Seinfeld, J. H. Representation of secondary organic aerosol laboratory chamber data for the interpretation of mechanisms of particle growth. *Environ. Sci. Technol.* **2005**, *39* (11), 4159−4165, DOI: 10.1021/es048292h.
(64) Coleman, B. K.; Lunden, M. M.; Destaillats, H.; Nazaroff, W. W. Secondary organic aerosol from ozone-initiated reactions with terpene-rich household products. *Atmos. Environ.* **2008**, *42* (35), 8234−8245, DOI: 10.1016/j.atmosenv.2008.07.031.
(65) Weschler, C. J.; Nazaroff, W. W. Semivolatile organic compounds in indoor environments. *Atmos. Environ.* **2008**, *42* (40), 9018−9040, DOI: 10.1016/j.atmosenv.2008.09.052.
(66) Larsen, B. R.; Di Bella, D.; Glasius, M.; Winterhalter, R.; Jensen, N. R.; Hjorth, J. Gas-phase OH oxidation of monoterpenes: Gaseous and particulate products. *J. Atmos. Chem.* **2001**, *38* (3), 231−276, DOI: 10.1023/a:1006487530903.
(67) Kroll, J. H.; Seinfeld, J. H. Chemistry of secondary organic aerosol: Formation and evolution of low-volatility organics in the atmosphere. *Atmos. Environ.* **2008**, *42* (16), 3593−3624, DOI: 10.1016/j.atmosenv.2008.01.003.
(68) Saltelli, A.; Ratto, M.; Tarantola, S.; Campolongo, F. Sensitivity analysis practices: Strategies for model-based inference. *Reliab. Eng. Syst. Safe.* **2006**, *91* (10−11), 1109−1125, http://dx.doi.org/10.1016/j.ress.2005.11.014.
(69) Jonsson, A. M.; Hallquist, M.; Ljungstrom, E. Influence of OH scavenger on the water effect on secondary organic aerosol formation from ozonolysis of limonene, Delta(3)-carene, and alpha-pinene. *Environ. Sci. Technol.* **2008**, *42* (16), 5938−5944, DOI: 10.1021/es702508y.